

Quantum Orbital Minimization Method for Excited States Calculation on Quantum Computer

Joel Bierman,[†] Yingzhou Li,^{*,‡} and Jianfeng Lu^{*,¶,†,§}

[†]*Department of Physics, Duke University*

[‡]*School of Mathematical Sciences, Fudan University*

[¶]*Department of Mathematics, Duke University*

[§]*Department of Chemistry, Duke University*

E-mail: yingzhouli@fudan.edu.cn; jianfeng@math.duke.edu

Abstract

We propose a quantum-classical hybrid variational algorithm, the quantum orbital minimization method (qOMM), for obtaining the ground state and low-lying excited states of a Hermitian operator. Given parameterized ansatz circuits representing eigenstates, qOMM implements quantum circuits to represent the objective function in the orbital minimization method and adopts classical optimizer to minimize the objective function with respect to the parameters in ansatz circuits. The objective function has orthogonality constraint implicitly embedded, which allows qOMM to apply a different ansatz circuit to each input reference state. We carry out numerical simulations that seek to find excited states of the H_2 and LiH molecules in the STO-3G basis and UCCSD ansatz circuits. Comparing the numerical results with existing excited states methods, qOMM is less prone to getting stuck in local minima and can achieve convergence with more shallow ansatz circuits.

1 Introduction

The development of quantum computing has boomed in recent years. The supremacy of quantum computing is demonstrated by sev-

eral groups.^{1,2} One of the most promising applications for noisy intermediate-scale quantum (NISQ) devices is the variational quantum eigensolver (VQE) under the full configuration interaction (FCI) framework.³⁻⁸ FCI is a quantum chemistry method which discretizes the time-independent many-body Schrödinger equation numerically exactly. The ground state and low-lying excited states are calculated via solving a standard eigenvalue problem, while the problem dimension scales exponentially as the number of electrons in the system. The FCI framework fits naturally into quantum computing. Quantum algorithms for ground state eigensolvers under FCI framework have been extensively developed in past decades.⁹⁻¹³ Among them, VQE is a quantum-classical hybrid method and has the shortest circuit depth, which makes it the most widely applied ground state quantum eigensolver on NISQ devices. In short, VQE adopts a parameterized circuit as the variational ansatz $|\phi_\theta\rangle$ for the ground state. Then the energy function $\langle\phi_\theta|\hat{H}|\phi_\theta\rangle$ is minimized with respect to the parameter θ , where \hat{H} is the Hamiltonian operator.

In addition to the ground state, excited states play an important role in connecting computational results and experimental observations in quantum chemistry. In this paper, we propose a hybrid quantum-classical algo-

rithm, named quantum orbital minimization method (qOMM), to compute the excited state energies as well as the corresponding states under FCI framework.

Existing approaches for excited states on quantum computers could be grouped into two categories: the excited state energy computation and the excited state vector computation.

Excited state energy computation on quantum computer evaluates the excited state energy without explicitly constructing the state vector. Two methods, quantum subspace expansion (QSE)¹⁴⁻¹⁶ and quantum equation of motion (qEoM),¹⁷ are representatives of this category. Both of them are based on perturbation theory starting from the ground state. They first construct the ground state $|\phi_{GS}\rangle$ via VQE. Then they evaluate the expansion values on single excited states from the ground state $|\phi_{GS}\rangle$, *i.e.*, $A_{p_1q_1}^{p_2q_2} = \langle \phi_{GS} | \hat{a}_{q_2}^\dagger \hat{a}_{p_2} \hat{H} \hat{a}_{p_1}^\dagger \hat{a}_{q_1} | \phi_{GS} \rangle$ and $B_{p_1q_1}^{p_2q_2} = \langle \phi_{GS} | \hat{a}_{q_2}^\dagger \hat{a}_{p_2} \hat{a}_{p_1}^\dagger \hat{a}_{q_1} | \phi_{GS} \rangle$ for \hat{a}_p^\dagger and \hat{a}_p being creation and annihilation operators. Once these expansion values are available, QSE solves a generalized eigenvalue problem of matrix pencil (A, B) and obtains the refined ground state energy and low-lying excited state energies on the perturbed space of $|\phi_{GS}\rangle$. qEoM adopts these expansion values into the equation of motion expression and obtains the low-lying excited state energies. Double excitations and higher order excitations from the ground state could be further evaluated and included to improve the accuracy of QSE and qEoM. However, including more excitations leads to a much higher computational cost.

Excited state vector computations include a wide spectrum of methods. Folded spectrum method¹⁸ folds the spectrum of a Hamiltonian operator via a shift-and-square operation, *i.e.*, $\hat{H} \rightarrow (\hat{H} - \lambda I)^2$, where λ is a chosen number close to the desired excited state energy. Then $(\hat{H} - \lambda I)^2$ is used as the operator in VQE method, and an excited state with the energy closest to λ is obtained via the optimization procedure in VQE. Witness-assisted variational eigenspectra solver^{19,20} adopts an entropy term as the regularizer in the objective function to keep the minimized excited state close to its ini-

tial state, where the initial state is set to be an excitation from the ground state. Quantum deflation method^{21,22} adopts the overlapping between the target state and the ground state as a penalty term in the objective function to keep the target state as orthogonal as possible to the ground state. The extension to more than one excited state in the quantum deflation method is straightforward. All these methods above have their classical algorithm counterparts. On the other hand, the following two methods use a unique property of quantum computing, *i.e.*, all quantum operators are unitary and orthogonal states after the actions of quantum operators are still orthogonal to each other. Subspace search VQE (SSVQE)²³ and multistate contracted VQE (MCVQE)²⁴ apply the same basic ansatz. They first prepare a sequence of non-parameterized mutually orthogonal states, $|\phi_1\rangle, |\phi_2\rangle, \dots, |\phi_K\rangle$ for K excited states. Then a parameterized circuit \hat{U}_θ is applied to these states, as \hat{U}_θ is unitary (implemented on a quantum computer), $\hat{U}_\theta |\phi_1\rangle, \dots, \hat{U}_\theta |\phi_K\rangle$ are mutually orthogonal. Hence we could minimize the objective function $\sum_k \langle \phi_k | \hat{U}_\theta^\dagger \hat{H} \hat{U}_\theta | \phi_k \rangle$ to obtain approximated ground state and excited states. While the energies associated with $\hat{U}_\theta |\phi_1\rangle, \dots, \hat{U}_\theta |\phi_K\rangle$ are usually not ordered. SSVQE further introduces a min-max problem to obtain a specific excited state. Also, in the SSVQE paper, a weighted objective function is employed to preserve the ordering, which will be referred to as weighted-SSVQE in our paper below. The MCVQE approach enriches the ansatz by introducing a unitary matrix applied across states, *i.e.*, $|\psi_k\rangle = \hat{U}_\theta \sum_\ell |\phi_\ell\rangle V_{\ell k}$ for $V_{\ell k}$ being the (ℓ, k) -th entry of a unitary matrix V . Hence a standard eigenvalue problem is solved as the post-processing in MCVQE to obtain V .

In this paper, we propose to obtain the excited state vector using the objective function in

the orbital minimization method (OMM),^{25,26}

$$f(|\psi_1\rangle, \dots, |\psi_K\rangle) = 2 \sum_{i=1}^K \langle \psi_i | \hat{H} | \psi_i \rangle - \sum_{i,j=1}^K \langle \psi_i | \psi_j \rangle \langle \psi_j | \hat{H} | \psi_i \rangle. \quad (1)$$

We refer our method as quantum orbital minimization method (qOMM) throughout this paper. An important property of (1) is that, even though the orthogonality conditions among $|\Psi_i\rangle$ s are not explicitly enforced, the minimizer of (1) consists of mutually orthogonal state vectors. While for most other methods, the orthogonality condition is explicitly proposed as a constraint in the optimization problem. The implicit orthogonality property allows us to adopt a different ansatz (with regards to either the numerical parameter values or the structure of the ansatz or both) for each excited state. In this paper, the largest variational ansatz class that we use is of the form,

$$|\tilde{\psi}_k\rangle = \sum_{\ell=1}^K \hat{U}_{\theta_\ell} |\phi_\ell\rangle V_{\ell k}, \quad (2)$$

where $|\phi_1\rangle, \dots, |\phi_K\rangle$ are initial states, $\hat{U}_{\theta_1}, \dots, \hat{U}_{\theta_K}$ are parameterized circuits with $\theta_1, \dots, \theta_K$ being the parameters, $V_{\ell k}$ is the (ℓ, k) -th entry of an invertible matrix V . Such an ansatz is richer than all ansatz used in other excited state vector methods. Another feature of (1) is that the objective function does not include any hyper-parameter (unlike, e.g., the deflation approach), which makes the method easy to use in practice without parameter tuning.

Notice that the objective function (1) includes the evaluation of the state inner product with respect to the Hamiltonian operator and the state inner product, *i.e.*, $\langle \phi_i | \hat{H} | \psi_j \rangle$ and $\langle \psi_i | \psi_j \rangle$, respectively. In other existing excited state methods, neither of these two are evaluated directly.¹ Given our variational ansatz,

¹In deflation method,^{21,22} the absolute value of the inner product, $|\langle \psi_i | \psi_j \rangle|$, is evaluated, while we need

we construct quantum circuits to evaluate both inner products, which are essentially inspired by the Hadamard test. When the evaluation of (1) is available on a quantum computer, we can adopt gradient-free optimizers to minimize the objective function with respect to parameters, $\theta_1, \dots, \theta_K$.

Finally, we include a sequence of numerical results to demonstrate the efficiency and robustness of the proposed method. Two chemistry systems, H_2 and LiH , at their equilibrium configurations are tested using the proposed method on quantum simulators. We observe that qOMM has two major benefits compared to algorithms such as weighted-SSVQE (In this paper, when we refer to SSVQE, we implicitly mean the weighted version of SSVQE that uses one optimization step for finding multiple eigenvalues simultaneously.) that enforce the orthogonality of the input states at every optimization step. 1) Enforcing the mutual orthogonality of the input states through the overlap terms allows for greater flexibility in the choice of ansatz applied to each input state, as well as greater flexibility in the choice of input states. The circuit applied to each input state must be identical in the SSVQE framework in order to enforce orthogonality, whereas qOMM allows us to apply a different ansatz circuit to each input state. 2) The tendency to get stuck in local minima, while not eliminated entirely, is diminished considerably. The first benefit is important since choosing a suitably expressive ansatz for excited states is often more difficult than the ground state VQE problem. In practice, this means that one is often able to use a more shallow and less expressive ansatz circuit; a feature that is crucial for applications on NISQ devices.

The rest of the paper is organized as follows. Section 2 illustrates the circuits we use to evaluate the inner products. The overall method is discussed in Section 3. In Section 4, we apply the method to various chemistry molecules to demonstrate the efficiency of the proposed method. Finally, Section 5 concludes the paper and discusses future work.

the actual value of the inner product without taking the absolute value.

2 Inner Product Circuits

In the objective function of qOMM, the inner product of two states and the inner product of two states with respect to an operator are complex numbers. Both the real and imaginary parts are explicitly needed to construct the objective function. If two states are identical, then the inner products can be efficiently evaluated by the well known Hadamard test. While if they are different, we propose quantum circuits for the evaluations of the inner products in this section.

To simplify the notations, we consider evaluating $\langle\psi|\phi\rangle$ and $\langle\psi|\widehat{H}|\phi\rangle$, where $|\psi\rangle$ and $|\phi\rangle$ are given by a unitary circuit acting on $|0\rangle$, *i.e.*, $|\psi\rangle = \widehat{U}_{\theta_\psi}|0\rangle$ and $|\phi\rangle = \widehat{U}_{\theta_\phi}|0\rangle$. Given the variational ansatz, the inner product $\langle\psi|\phi\rangle = \langle 0|\widehat{U}_{\theta_\psi}^\dagger\widehat{U}_{\theta_\phi}|0\rangle$ can be viewed as the inner product of $|0\rangle$ with respect to the operator $\widehat{O} = \widehat{U}_{\theta_\psi}^\dagger\widehat{U}_{\theta_\phi}$. In principle, the transpose of the ansatz circuit can be constructed. After the ansatz circuit is compiled into basic gates, the transpose of the circuit is the composition of the

transposed basic gates in the reverse ordering. Hence $\langle\psi|\phi\rangle$ could be then evaluated using the Hadamard test, which requires the controlled ansatz circuit and the controlled transpose of the ansatz circuit. Instead, we adopt an idea inspired by the Hadamard test, which can be applied to evaluate $\langle\psi|\widehat{H}|\phi\rangle$ without controlled transpose of the ansatz circuit. In the following, we discuss such two quantum circuits evaluating the inner products in detail.

2.1 $\langle\psi|\phi\rangle$ evaluation

For complex-valued states $|\psi\rangle$ and $|\phi\rangle$, the inner product $\langle\psi|\phi\rangle$ is also a complex number. The evaluation of $\langle\psi|\phi\rangle$ is divided into the evaluations of the real and imaginary parts. We will introduce the circuit for evaluation of the real part of $\langle\psi|\phi\rangle$ in detail, and the circuit for the imaginary part could be constructed analogously.

Figure 1 illustrates the precise quantum circuit used to evaluate the real part of $\langle\psi|\phi\rangle$. Here we list expressions at all five stages as shown in the figure:

$$(H \otimes I) |0\rangle |\vec{0}\rangle = \frac{1}{\sqrt{2}} (|0\rangle + |1\rangle) |\vec{0}\rangle, \quad (\text{S}_1)$$

$$C\text{-}\widehat{U}_{\theta_\phi} \frac{1}{\sqrt{2}} (|0\rangle + |1\rangle) |\vec{0}\rangle = \frac{1}{\sqrt{2}} (|0\rangle |\vec{0}\rangle + |1\rangle |\phi\rangle), \quad (\text{S}_2)$$

$$(X \otimes I) \frac{1}{\sqrt{2}} (|0\rangle |\vec{0}\rangle + |1\rangle |\phi\rangle) = \frac{1}{\sqrt{2}} (|1\rangle |\vec{0}\rangle + |0\rangle |\phi\rangle), \quad (\text{S}_3)$$

$$C\text{-}\widehat{U}_{\theta_\psi} \frac{1}{\sqrt{2}} (|1\rangle |\vec{0}\rangle + |0\rangle |\phi\rangle) = \frac{1}{\sqrt{2}} (|1\rangle |\psi\rangle + |0\rangle |\phi\rangle), \quad (\text{S}_4)$$

$$(H \otimes I) \frac{1}{\sqrt{2}} (|1\rangle |\psi\rangle + |0\rangle |\phi\rangle) = \frac{1}{2} (|0\rangle (|\phi\rangle + |\psi\rangle) + |1\rangle (|\phi\rangle - |\psi\rangle)), \quad (\text{S}_5)$$

where H is the Hadamard gate, X is the Pauli-X gate, I is the identity mapping, $C\text{-}\widehat{U}$ is the controlled \widehat{U} gate. Conducting the measurement on the ancilla qubit, we have the prob-

ability measuring zero being,

$$\begin{aligned} \mathbb{P}(\text{measurement} = 0) &= \frac{1}{4} (\langle\phi| + \langle\psi|) (|\phi\rangle + |\psi\rangle) \\ &= \frac{1}{2} + \frac{1}{2} \text{Re} \langle\psi|\phi\rangle, \end{aligned} \quad (3)$$

where $\text{Re}(\cdot)$ denotes the real part of the complex number. Hence, if we execute the quantum circuit as in Figure 1 for M shots and count the number of zeros, the $\text{Re} \langle \psi | \phi \rangle$ could be well-approximated given M is reasonably large.

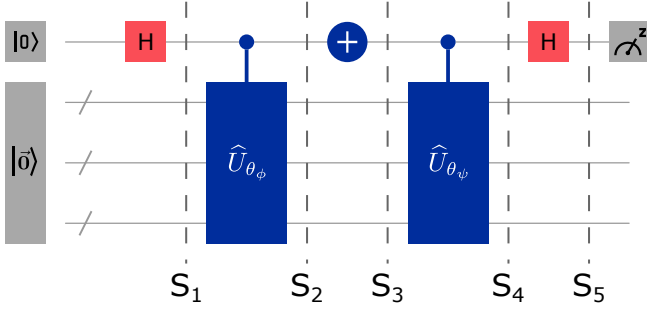


Figure 1: Inner product circuit.

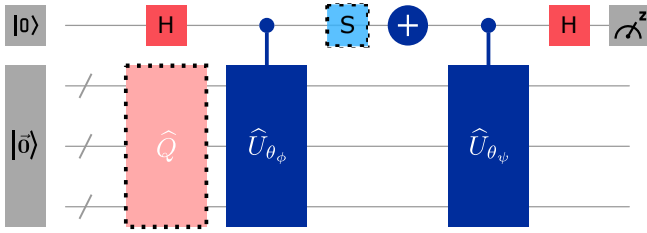


Figure 2: Extended inner product circuit.

The imaginary part of $\langle \psi | \phi \rangle$ could be estimated in a similar way. Notice that the real part in (3) comes from $\langle \psi | \phi \rangle + \langle \phi | \psi \rangle$. If either $|\psi\rangle$ or $|\phi\rangle$ is replaced by $i|\psi\rangle$ or $i|\phi\rangle$, then the real part in (3) corresponds to the imaginary part of the inner product instead. One way to implement the replacement is to add a phase gate on the ancilla qubit after stage (S_2). The resulting quantum circuit is as that in Figure 2 where the light blue dash box is enabled. We then need to execute the circuit for another M shots to obtain the approximation of $\text{Im} \langle \psi | \phi \rangle$.

In addition to variational ansatz $|\psi\rangle = \hat{U}_{\theta_\psi} |0\rangle$ and $|\phi\rangle = \hat{U}_{\theta_\phi} |0\rangle$, we could extend the quantum circuit to variational ansatz $|\psi\rangle = \hat{U}_{\theta_\psi} \hat{Q} |0\rangle$ and $|\phi\rangle = \hat{U}_{\theta_\phi} \hat{Q} |0\rangle$, where \hat{Q} is a common quantum circuit preparing the initial state. If such ansatz are adopted, we could enable the light pink dash box in Figure 2 such that the circuit \hat{Q} is applied on $|0\rangle$ as a common circuit. The real and imaginary parts of the inner product are evaluated similarly as before.

2.2 $\langle \psi | \hat{H} | \phi \rangle$ evaluation

The Hamiltonian operator considered in this paper is under FCI framework and admits the form,

$$\hat{H} = \sum_{p,q=1}^{N_{\text{orb}}} h_{pq} \hat{a}_p^\dagger \hat{a}_q + \sum_{p,q,r,s=1}^{N_{\text{orb}}} v_{pqrs} \hat{a}_p^\dagger \hat{a}_q^\dagger \hat{a}_s \hat{a}_r, \quad (4)$$

where h_{pq}, v_{pqrs} are one-body and two-body integrals respectively. The Hamiltonian operator \hat{H} , in general, is not a unitary operator. Hence, it cannot be represented by a quantum circuit directly. On the other hand, the excitation operators, $\hat{a}_p^\dagger \hat{a}_q$ and $\hat{a}_p^\dagger \hat{a}_q^\dagger \hat{a}_s \hat{a}_r$, are unitary and can be represented by quantum circuits. The detailed circuits of these excitation operators depend on the encoding scheme. All methods proposed in this paper do not rely on the encoding scheme and we use Jordan-Wigner encoding for all numerical examples. The value $\langle \psi | \hat{H} | \phi \rangle$ is then calculated as a weighted summation of circuit results,

$$\begin{aligned} \langle \psi | \hat{H} | \phi \rangle &= \sum_{p,q=1}^{N_{\text{orb}}} h_{pq} \langle \psi | \hat{a}_p^\dagger \hat{a}_q | \phi \rangle \\ &+ \sum_{p,q,r,s=1}^{N_{\text{orb}}} v_{pqrs} \langle \psi | \hat{a}_p^\dagger \hat{a}_q^\dagger \hat{a}_s \hat{a}_r | \phi \rangle. \end{aligned} \quad (5)$$

Thus it suffices to consider circuits for the evaluation of $\langle \psi | \hat{U} | \phi \rangle$, where \hat{U} denotes a general unitary operator.

Figure 3 illustrates the circuit for $\langle \psi | \hat{U} | \phi \rangle$. This circuit can be understood in the same way as the circuit of $\langle \psi | \phi \rangle$. The value $\langle \psi | \hat{U} | \phi \rangle$ can be explicitly written as,

$$\langle \psi | \hat{U} | \phi \rangle = \left(\langle 0 | \hat{U}_{\theta_\psi}^\dagger \right) \left(\hat{U} \hat{U}_{\theta_\phi} | 0 \rangle \right) = \langle \psi | \tilde{\phi} \rangle, \quad (6)$$

where the construction circuit for $|\tilde{\phi}\rangle$ is $\hat{U} \hat{U}_{\theta_\phi}$. Hence Figure 3 is essentially the circuit in Figure 1 and Figure 2 with a modified constructing circuit for $|\phi\rangle$.

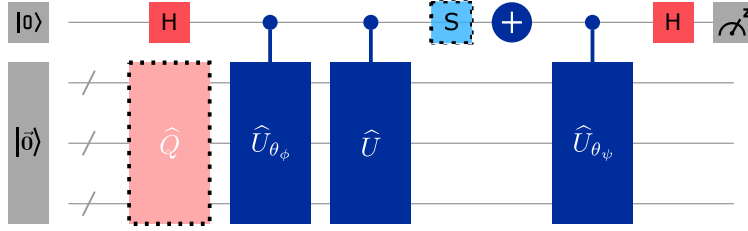


Figure 3: Extended inner product circuit with a unitary gate.

3 Quantum Orbital Minimization Method

Orbital minimization method originates in the field of density functional theory (DFT). The minimization problem admits the following linear algebra form,

$$\min_{X \in \mathbb{C}^{N \times K}} \text{tr}((2I - X^*X)X^*\hat{H}X), \quad (7)$$

where X is a multi-column vectors with each column denoting a state vector, \hat{H} is abused to be the Hamiltonian matrix, I is the identity matrix of size $K \times K$, and $\text{tr}(\cdot)$ denotes the trace operator. When \hat{H} is Hermitian negative definite, all local minima of (7) are of the form,²⁷

$$X = QV, \quad (8)$$

where $Q \in \mathbb{C}^{N \times K}$ are K eigenvectors of \hat{H} associated with the smallest K eigenvalues, and $V \in \mathbb{R}^{K \times K}$ is an arbitrary unitary matrix. Substituting (8) back into (7), we find that all these local minima are of the same objective value and they are global minima. Unlike many other optimization problems for solving the low-lying eigenvalue problem, OMM as in (7) does not have any explicit orthogonal constraint and the orthogonality in (8) could be achieved without any orthogonalization step. This property is the key reason for us to investigate the application of (7) in quantum computing, where explicit orthogonalization is difficult to implement in the presence of hardware and environmental noise.

In the quantum computing setting, each column of X is represented by the ansatz $|\psi_i\rangle = \hat{U}_{\theta_i}|\phi_i\rangle$. By the nature of quantum computing, if quantum error is not taken into account, $|\psi_i\rangle$ is always of unit length for all i . Hence the

$2I - X^*X$ term in (7) has one on its diagonal. Substituting the variational ansatz into (7), we obtain the optimization problem for our quantum excited state problem,

$$\min_{\theta_1, \dots, \theta_K} g(\theta_1, \dots, \theta_K) \quad (9)$$

for

$$\begin{aligned} &g(\theta_1, \dots, \theta_K) \\ &= \sum_{i=1}^K \langle \phi_i | \hat{U}_{\theta_i}^\dagger \hat{H} \hat{U}_{\theta_i} | \phi_i \rangle \\ &\quad - \sum_{\substack{i,j=1 \\ i \neq j}}^K \langle \phi_i | \hat{U}_{\theta_i}^\dagger \hat{U}_{\theta_j} | \phi_j \rangle \langle \phi_j | \hat{U}_{\theta_j}^\dagger \hat{H} \hat{U}_{\theta_i} | \phi_i \rangle. \end{aligned} \quad (10)$$

If the variational space is rich enough such that vectors in QV as in (8) can be well-approximated by $\{\hat{U}_{\theta_i}|\phi_i\rangle\}_{i=1}^K$, then qOMM can achieve a good approximation to the global minimum of its linear algebra counterpart (7). In practice, if we obtain the global minimum value of (7) for qOMM (though the value is not known in advance), then we are confident that the ansatz is rich enough and the optimizer works perfectly in finding the global minimum for parameters $\theta_1, \dots, \theta_K$. However, we lack the theoretical understanding of the energy landscape of (9). In part, the dependence of g on $\theta_1, \dots, \theta_K$, like that in the deep neural network, is highly nonlinear and nonconvex. It could be analyzed for some simple ansatz circuit. However, for most complicated circuits, the analysis remains difficult. On the other hand, from the linear algebra point of view, when the variational space is rich enough, we could view the problem as optimizing the vectors X directly in (7). The nature of quantum computer poses

unit length constraints on each column of X . Adding extra unit length constraints would dramatically change the energy landscape of the original problem (7). We defer the theoretical understanding of (9) to future work. In this pa-

per, we focus on the numerical performance of (9).

For numerical optimization of the objective function g , note that its gradient with respect to a parameter $\theta_{i\alpha}$ is given by

$$\begin{aligned} \frac{dg}{d\theta_{i\alpha}} = & 2 \operatorname{Re} \left\langle \phi_i \left| \frac{d\widehat{U}_{\theta_i}^\dagger}{d\theta_{i\alpha}} \widehat{H} \widehat{U}_{\theta_j} \right| \phi_j \right\rangle - 2 \operatorname{Re} \sum_{\substack{j=1 \\ j \neq i}}^K \left\langle \phi_i \left| \frac{d\widehat{U}_{\theta_i}^\dagger}{d\theta_{i\alpha}} \widehat{U}_{\theta_j} \right| \phi_j \right\rangle \left\langle \phi_j \left| \widehat{U}_{\theta_j}^\dagger \widehat{H} \widehat{U}_{\theta_i} \right| \phi_i \right\rangle \\ & - 2 \operatorname{Re} \sum_{\substack{j=1 \\ j \neq i}}^K \left\langle \phi_i \left| \widehat{U}_{\theta_i}^\dagger \widehat{U}_{\theta_j} \right| \phi_j \right\rangle \left\langle \phi_j \left| \widehat{U}_{\theta_j}^\dagger \widehat{H} \frac{d\widehat{U}_{\theta_i}}{d\theta_{i\alpha}} \right| \phi_i \right\rangle, \end{aligned} \quad (11)$$

where $\theta_{i\alpha}$ is the α -th parameter in θ_i . From (11), we notice that the gradient evaluation requires an efficient quantum circuit for $\frac{d\widehat{U}_{\theta_i}}{d\theta_{i\alpha}}$. The existence of such quantum circuits is ansatz dependent. Assume that we can evaluate (11) for all parameters. Then the update on parameters follows a gradient descent method as

$$\theta^{(t+1)} = \theta^{(t)} - \tau \nabla_{\theta} g(\theta^{(t)}),$$

for $\theta^{(t+1)}$ and $\theta^{(t)}$ being all parameters at $(t+1)$ -th and (t) -th iteration respectively, and τ is the stepsize. Since all evaluations of quantum circuits involve randomness, in practice, this amounts to using the stochastic gradient descent method. Other advanced first order methods recently developed in deep neural network literature, *e.g.*, ADAM, AdaGrad, coordinate descent method, etc., could be used to accelerate. These methods could achieve better performance than the vanilla stochastic gradient descent method.

When the gradient circuit is not available, we can adopt zeroth-order optimizers to solve (9). In this work, we use L-BFGS-B²⁸ as the optimizer, which uses a 2-point finite difference gradient approximation and thus does not require explicit implementation of the circuit for $\frac{d\widehat{U}_{\theta_i}}{d\theta_{i\alpha}}$. We find this optimizer to work well in the noiseless simulations we consider here, but

we note that other promising candidates for noisy simulations and experimental calculations exist, which could also be used for our proposed objective function. In particular, using simultaneous perturbation stochastic approximation (SPSA) for small molecule VQE calculations has been demonstrated experimentally on superconducting hardware²⁹ and a quantum natural gradient version of SPSA also exists.³⁰

When the optimization problem is solved, we will obtain a set of parameters $\theta_1, \dots, \theta_K$ such that $\widehat{U}_{\theta_1} |\phi_1\rangle, \dots, \widehat{U}_{\theta_K} |\phi_K\rangle$ approximate vectors in QV as in (8). Numerically, we find that V is very close to an identity matrix, while a post-processing procedure still improves the accuracy of the approximation. The post-processing procedure is slightly different from that in MCVQE. We construct two matrices with their (i, j) -th elements being,

$$\begin{aligned} A_{ij} &= \left\langle \phi_i \left| \widehat{U}_{\theta_i}^\dagger \widehat{H} \widehat{U}_{\theta_j} \right| \phi_j \right\rangle \text{ and} \\ B_{ij} &= \left\langle \phi_i \left| \widehat{U}_{\theta_i}^\dagger \widehat{U}_{\theta_j} \right| \phi_j \right\rangle. \end{aligned} \quad (12)$$

Then a generalized eigenvalue problem with matrix pencil (A, B) is solved as,

$$AR = BR\Lambda, \quad (13)$$

where R denotes the eigenvectors and Λ is a diagonal matrix with eigenvalues of (A, B) being

its diagonal entries. The desired eigenvalues of \hat{H} are in Λ and the corresponding eigenvectors admits $\sum_{j=1}^K \hat{U}_{\theta_j} |\phi_j\rangle R_{ji}$ for $i = 1, \dots, K$. The eigenvector, which is the excited state of \hat{H} , can be explicitly constructed as a linear combination of unitary operators³¹ on a quantum computer.

qOMM has its unique features comparing to existing excited state vector methods. The targets of folded spectrum method¹⁸ and witnessing eigenspectra solver^{19,20} are different from that of qOMM. Quantum deflation method^{21,22} addresses the excited states one-by-one, and the optimization problems therein are of different difficulty as that in qOMM. The most related excited state vector methods to qOMM are SSVQE and MCVQE. Since SSVQE and MCVQE are very similar to each other, we focus on the difference among qOMM and SSVQE in this paper. Both the qOMM and weighted SSVQE algorithm²³ take a set of input states and seek to simultaneously optimize the parameterized circuit and obtain the low-lying eigenvalues and eigenvectors of the Hermitian operator. Both methods achieve their goal via solving a single optimization problem. There are two major differences between them. The first one is how the mutual orthogonality of the eigenvectors is enforced. The construction of the weighted SSVQE objective function ensures that the set of states being evaluated is mutually orthogonal throughout optimization iteration. The proposed qOMM implicitly embeds this constraint into the objective function such that the states being evaluated are only guaranteed to be mutually orthogonal at the global minimum. The first difference leads to the second major difference. SSVQE adopts the ansatz circuits for different states that must admit mutual orthogonal property. Hence, they restrict their ansatz circuits to be a set of identical parameterized circuits acting on mutually orthogonal initial states. qOMM does not constrain the ansatz circuits in this way. qOMM could adopt as its set of parameterized circuits any combination of ansatz circuits that have been tested in the literature, *e.g.*, ansatz circuits in MCVQE²⁴ and SSVQE,²³ ansatz circuits in de-

flation method,^{21,22} etc. In addition to these ansatz circuits, qOMM could also adopt other ansatz circuits not been tested by excited state methods. In this work, we adopt UCCSD³² as our main ansatz circuit so that the particle number is preserved throughout.

4 Numerical Results

We present the numerical results of our proposed method obtained from a classically simulated noiseless quantum computer. We apply it to the problem of finding low-lying eigenvalues of the electronic structure Hamiltonian for near-equilibrium configurations of two different molecules. While interesting future works could include studying the performance in settings that include noise, *i.e.*, on an actual quantum device or on a classical simulation with a noise model. The goal here is to illustrate the “best-case scenario” performance. Thus, the numerical tests in this section serve to explore what advantages or disadvantages may arise for each of the qOMM and weighted SSVQE approaches (using weight vectors of the form $[n, n - 1, \dots, 1]$ for finding n states) in different situations.

All codes for these simulations are implemented using the Qiskit³³ library. The electronic structure Hamiltonians were generated using molecular data from PySCF³⁴ in the STO-3G basis and mapped to qubit Hamiltonians using the Jordan-Wigner mapping. The relative accuracies of the results for both methods are calculated by comparing them to their numerically exact counterparts obtained by numerically exact diagonalization of the Hamiltonians. Simulations for finding the energy levels of H_2 were performed at an interatomic distance of 0.735 Angstroms, and those of LiH were performed at an interatomic distance of 1.595 Angstroms. For the LiH simulations, we freeze the two core electrons to reduce the problem size from 12 qubits to 10 qubits.

The set of initial states for both algorithms and molecular Hamiltonians were chosen to be the Hartree-Fock state and low-lying single-particle excitations above it. For example, if we wish to find three energy levels for 4-

qubit H_2 , this would be the set: $\{|01\rangle_\alpha |01\rangle_\beta, |01\rangle_\alpha |10\rangle_\beta, |10\rangle_\alpha |01\rangle_\beta\}$. For LiH, this would be the set: $\{|00001\rangle_\alpha |00001\rangle_\beta, |00001\rangle_\alpha |00010\rangle_\beta, |00010\rangle_\alpha |00001\rangle_\beta\}$, where the subscript α and β denote the spin group ². Given that the UCCSD³² ansatz preserves the numbers of spin-up and spin-down, the above choice of initial states constrains these variational quantum algorithms to search only the desired subspace, lessening the computational difficulty and producing physically meaningful results at the same time. For this reason, UCCSD is our ansatz of choice for these simulations. If we wish to find only two energy levels, we would omit the highest-energy state from the set. This choice of the set of states allows us to study two different types of algorithm initializations: one in which all of the ansatz parameters are randomly sampled according to a uniform distribution on $[-2\pi, 2\pi)$ and another one in which they are all set to zero. With the random parameter initialization, we can study the robustness of the algorithms with respect to their starting point in the parameter space. With the “zero vector” initialization, the UCCSD ansatz circuit is initialized to the identity and the states after the initial ansatz circuit application remain the Hartree-Fock state and low-lying single-particle excitations above the Hartree-Fock states. For most molecules, these states from Hartree-Fock calculation are good approximations of the ground state and low-lying excited states under FCI. So the optimization from the “zero vector” initialization could be viewed as a local optimization and improves the performance of optimizers upon the random initialization. In Qiskit’s implementation of ansatz circuits such as UCCSD, one can increase the expressiveness of the ansatz by repeating the corresponding quantum circuit block pattern r times, which comes at the cost of both the circuit depth and the number of

²In the Qiskit implementation of n -qubit basis states in the Jordan-Wigner representation, the first $\frac{n}{2}$ qubits encode spin-up (α) and the second $\frac{n}{2}$ qubits encode spin-down (β). Thus we have chosen these three basis states because they are elements of the 2-particle, spin magnetization $S_z = 0$ subspace of the full 2^n -dimensional Fock space.

variational parameters increasing by a factor of r . In this paper, we refer to an ansatz circuit that consists of the UCCSD circuit block pattern repeated r times as r -repetition UCCSD (or simply r -UCCSD). We run both algorithms for several different numbers of repetitions in order to account for the fact that the necessary ansatz expressiveness for convergence is not known *a priori*. Such a study allows us to explore the dependence of convergence success on the circuit depth for each algorithm.

When using a random initialization, we run each algorithm ten times for each setting and plot the objective convergence for all ten runs. When using the “zero vector” initialization, we run each algorithm only once. Running the algorithm multiple times for this initialization is neither necessary nor useful in the absence of noise since the outcome is deterministic for a given initial point.

4.1 H_2

We begin by presenting the results for the 4 qubit system we consider here: H_2 . Figure 4 and Figure 5 illustrate the convergence of the objective function for each algorithm when attempting to calculate the first three energy levels of the H_2 molecule.

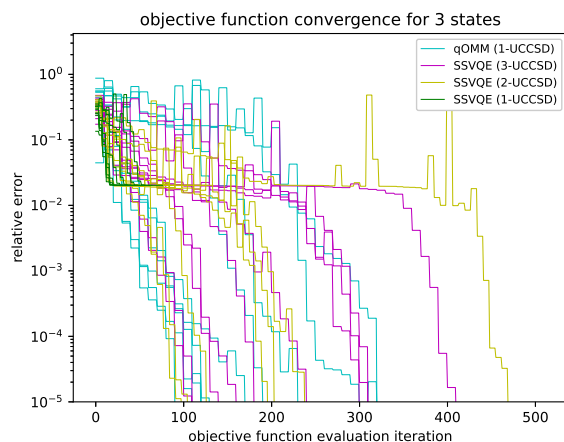


Figure 4: Convergence of qOMM and SSVQE for three H_2 states using a random parameter initialization and the L-BFGS-B optimizer.

Figure 4 illustrates how qOMM and SSVQE both converge to the global minimum, but

Table 1: The success rate for a given problem instance converges to within a relative accuracy of 10^{-5} for a given number of UCCSD repetitions using a randomized ansatz parameter initialization.

Molecule	Algorithm	UCCSD Repetitions		
		1-rep	2-rep	3-rep
H ₂	qOMM (3 states)	100%	–	–
	SSVQE (3 states)	0%	70%	100%
LiH	qOMM (2 states)	0%	100%	–
	SSVQE (2 states)	0%	80%	–
	qOMM (3 states)	0%	100%	–
	SSVQE (3 states)	0%	0%	70%

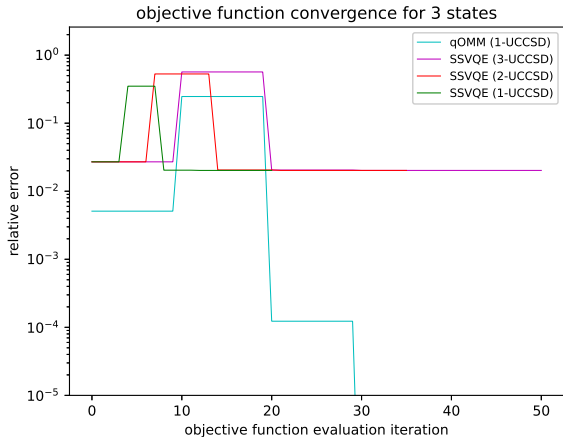


Figure 5: Convergence of qOMM and SSVQE for three H₂ states using the zero vector parameter initialization and the L-BFGS-B optimizer.

notably, SSVQE cannot do so with just 1-repetition UCCSD, requiring two repetitions in order to converge to within a relative accuracy of 10^{-5} . The success rate is further reported in Table 1. Figure 5 illustrates an attempt to solve the same problem, except the ansatz parameters are all initialized to zero. In this instance, we see that qOMM converges more quickly by a factor in the range of 3-10 compared to its random initialization counterpart, while SSVQE gets stuck in a local minimum and does not converge regardless of the ansatz circuit depth used. In both figures and all later convergence figures in this paper, we depict the convergence curve as the relative error against the number of the objective function evaluations, which is considered the most expensive operation in VQE-type algorithms. The L-BFGS-B imple-

mentation used in this paper uses a 2-point finite difference method such that each parameter is perturbed slightly from a given reference point common to all of them. Thus for an n -parameter objective function, $n + 1$ function evaluations are required for each parameter update step in order to estimate the gradient. Hence, in all convergence figures, we observe stair-like curves of width $n + 1$.

4.2 LiH

We now present the results for the 10-qubit system we consider here: LiH. Many settings are tested on LiH system. Figure 6a and Figure 6b illustrate the convergence of the objective function for both algorithms with various UCCSD ansatzes when calculating the lowest two energy levels. Figure 7a and Figure 7b illustrate the convergence of qOMM and SSVQE when attempting to find the lowest three energy levels.

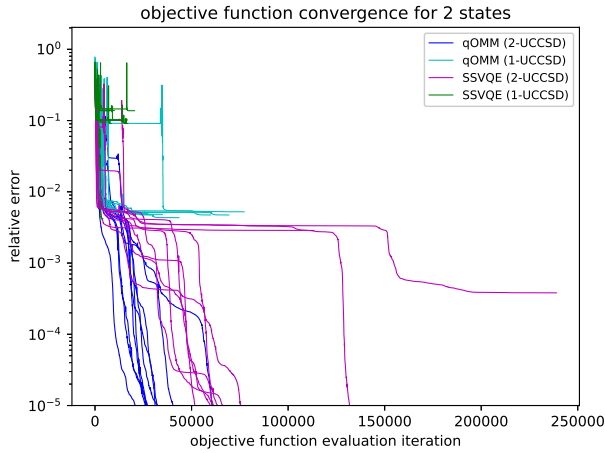
We can see from Figure 6a that when the ansatz parameters are randomly initialized, both algorithms demonstrate the ability to converge within an accuracy of 10^{-5} , but require 2-repetition UCCSD to do so. From Figure 6b we can see that when all of the parameters are initialized to zero, both algorithms converge to within a relative accuracy of 10^{-5} much more quickly than their randomly initialized counterparts. Notably, qOMM requires only 1-repetition UCCSD to achieve this convergence, while SSVQE requires two repetitions. When three states are calculated (see Figure 7), the

results here are similar to that of finding two states, but at the cost of more function evaluations. qOMM can achieve a convergence below 10^{-5} with 2-repetition UCCSD, whereas SSVQE requires three repetitions. From Figure 7b we can see that when the ansatz parameters are all initialized to zero, both algorithms quickly converge to the global minimum. Notably, qOMM requires only 1 UCCSD repetition with this initialization.

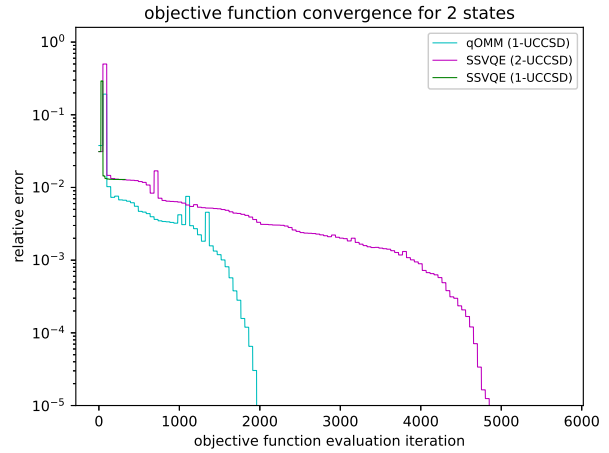
In the following, we discuss the numerical results on LiH mainly from three perspectives: convergence plateau, initialization, and ansatz circuit depth.

Convergence Plateau. In almost all LiH convergence plots we show here, both qOMM and SSVQE initially converge at a rapid rate but then hit a plateau and stall the convergence until they escape from the “bad” region of the energy landscape. As long as the algorithm escapes from the “bad” region, the convergence rate resumes being rapid. These “bad” regions of the energy landscape (regardless of what their nature may be) seem to be the main obstacle for the convergence of both algorithms, which is more severe to SSVQE. Studying this apparent feature of the energy landscape may provide some insight as to how both algorithms may be improved and what limitations are inherent to the construction of the cost functions. From a numerical linear algebra point of view, such a convergence behavior is not very surprising. The objective function in SSVQE is convex. While, with the consideration of the orthogonality constraint and the parameterization of the ansatz circuits, the energy landscape of SSVQE becomes non-convex. On the other hand, the objective function of qOMM, by itself, is non-convex but has no spurious local minima.^{27,35,36} When the parameterization of the ansatz circuits is taken into consideration, the energy landscape of qOMM is non-convex and could have spurious local minima. For non-convex energy landscapes, usual optimizers, including L-BFGS-B, are efficient in a neighborhood of local minima whereas, around strict saddle points, without second-order information, the optimizers could stall there for a long time. From a practical point of view,

we can further investigate the convergence of each eigenvalue. Since the issue is more severe for SSVQE, we focus on the SSVQE rather than qOMM. The construction of the SSVQE objective function allows us to obtain the estimated values for each eigenvalue at every function evaluation (in addition to the objective function as a whole) at a negligible additional computational cost. This allows us to gain some intuition as to why the SSVQE objective function convergence is observed to plateau in most of the LiH runs before steeply converging below a relative accuracy of 10^{-5} . In Figure 8 and Figure 9, we plot the eigenvalues and their relative accuracies, respectively, for one of the ten randomly-initialized SSVQE runs displayed in Figure 7a. We can see from Figure 8 that while E_0 converges rapidly, the convergence of E_1 and E_2 plateau and do not converge for many more function evaluations. From Figure 9 we can see that E_1 does not escape from its plateau until the accuracy of E_0 is sufficiently decreased. This is followed by the accuracies of E_0 and E_1 increasing together. E_2 does not escape from its plateau until the accuracies of E_0 and E_1 are both sufficiently decreased, after which the accuracies of all three energy levels collectively increase, allowing the objective function to converge to its global minimum. While we only illustrate this for one of the ten runs in Figure 7a, we observe that this qualitative behavior is typical for the other nine runs. Besides the non-convexity reason from objective functions, other reasons for this behavior could be related to two aspects of the weighted sum nature of the SSVQE algorithm. First, the same ansatz circuit is applied to all input states, meaning any change in the parameters has a direct impact on all the expectation value terms simultaneously. Second, the energy levels contribute unequally to the overall cost function, with the lower energy levels contributing more than the higher energy levels, an effect that becomes more pronounced due to the presence of the weight vector. Because qOMM enforces orthogonality (at the global minimum) through its overlap terms, the energy expectation value terms are associated with different independent parameter values. This means that changes in parameters

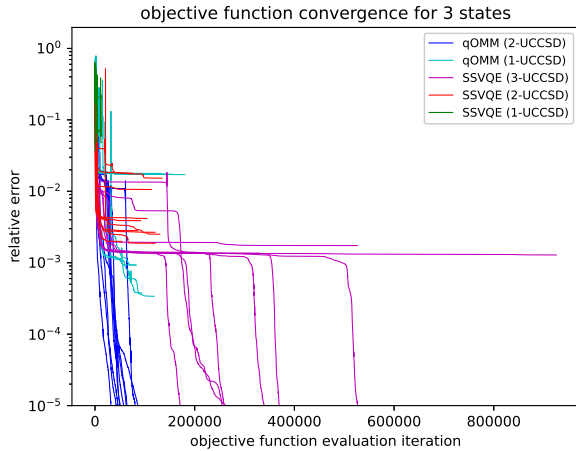


(a) Random parameter initialization

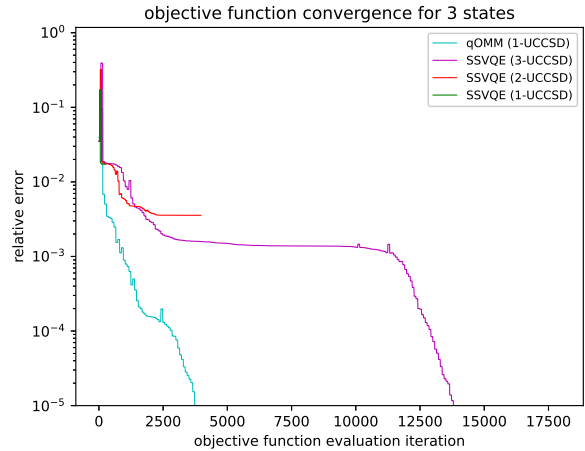


(b) Zero vector parameter initialization

Figure 6: Convergence of qOMM and SSVQE for two LiH states using the L-BFGS-B optimizer.



(a) Random parameter initialization



(b) Zero vector parameter initialization

Figure 7: Convergence of qOMM and SSVQE for three LiH states using the L-BFGS-B optimizer.

that directly affect one of the energy expectation value terms in (1) do not directly change the others. They only change the overlap terms. This affords qOMM a flexibility that allows it to spend much fewer iterations escaping from the “bad” landscape regions. From Figure 7b and Figure 6b we see that starting with a good initial guess can reduce this effect, resulting in significantly improved convergence.

Initialization. Initialization plays an important role in the convergence for both qOMM and SSVQE. Even for the corresponding VQE ground state problem with 1-repetition UCCSD, as in Figure 10, random parameter initialization on average converges in about

100 times more objective function evaluations than the zero vector parameter initialization. Both initializations in Figure 10 converge to a relative error 10^{-5} . In excited state computing, the two different initialization strategies for both qOMM and SSVQE not only differ in the number of iterations but also differ in the convergence results. Comparing two figures in Figure 6, for SSVQE with 2-repetition UCCSD, random parameter initialization converges more than ten times slower than that of zero vector parameter initialization. A similar result can be observed in Figure 7 for SSVQE with 3-repetition UCCSD. Besides the difference in the number of iterations, optimiza-

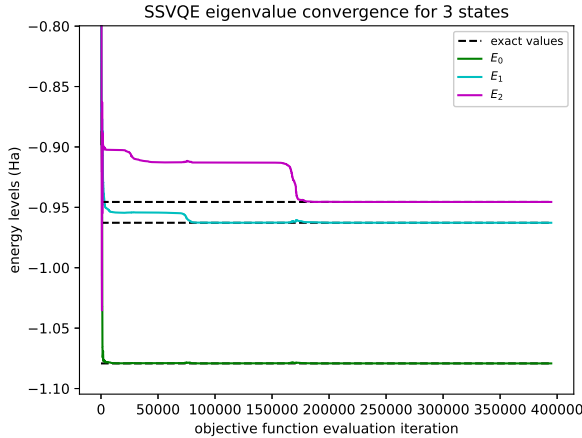


Figure 8: Convergence of the first three energy levels of LiH for SSVQE using the L-BFGS-B optimizer and a random parameter initialization.

tion starting from random parameter initializations sometimes cannot find the global minima. In Figure 6b, both qOMM with 1-repetition UCCSD and SSVQE with 3-repetition UCCSD converge to global minima while their random parameter initialization counterparts in Figure 6a behave differently. As summarized in Table 1, for SSVQE, two out of ten random initializations fail to converge to the global minima. For qOMM, all ten random initializations fail. Similar behaviors in Figure 7 can be observed for qOMM with 1-repetition UCCSD and SSVQE with 3-repetition UCCSD. Overall, in all results included in this paper, zero vector parameter initializations outperform their random parameter initialization counterparts for both algorithms. However, we still include numerical results for random parameter initializations to demonstrate the different performance between qOMM and SSVQE. This is because the zero vector initializations initialize the states to be excitations from Hartree-Fock states and only work for a limited number of low-lying states. If more excited states are needed, the zero vector initialization could even be a bad initialization, which is due to the fact that the excitation energies from Hartree-Fock may not be in the consistent order with that of FCI excitation energies. This "zero vector" initialization is demonstrated primarily not to

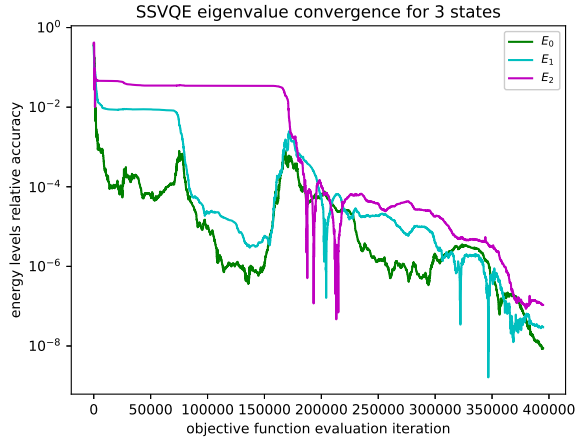


Figure 9: Relative accuracy of the convergence of the first three energy levels of LiH for SSVQE using the L-BFGS-B optimizer and a random parameter initialization.

advocate for its use as a scalable initialization strategy, but to illustrate what the improved convergence could look like if it can be assumed that one has a reasonable initialization strategy. The flexibility of variational ansatzes in qOMM would have another advantage when many excited states are needed. In qOMM, we could use zero vector parameter initialization for a few states and random parameter initialization for the remaining states without known good initializations. Such a mixed initialization strategy could avoid being trapped in bad local minima and benefit from the fast convergence of those states with zero vector parameter initialization. SSVQE, unfortunately, cannot use such a mixed initialization strategy due to the implicit orthogonality among initialized states. This motivates further investigation into developing and benchmarking initialization strategies more sophisticated than the ones we consider in this work.

Ansatz Circuit Depth. Based on our numerical results, increasing the ansatz circuit depth, *i.e.*, increasing the repetition in UCCSD, has two major impacts. First, the expressiveness increases as the ansatz circuit depth increases. In the ground state VQE, as in Figure 10, 1-repetition UCCSD is sufficient for the ansatz to approximate the ground state to chemical accuracy. When two states of LiH are needed,

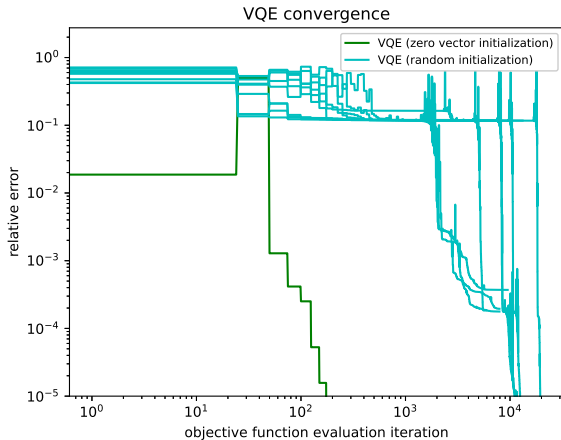


Figure 10: Convergence of VQE for the ground state problem of LiH using a random parameter initialization and the L-BFGS-B optimizer.

1-repetition UCCSD, as in Figure 6, is not able to simultaneously approximate the ground state and the first excited states, whereas 2-repetition UCCSD is able to. From the qOMM results in Figure 6, we know that 1-repetition UCCSD is able to approximate the ground state and the first excited state. When three states are needed, as in Figure 7, we need 3-repetition UCCSD to simultaneously approximate three states. Again, 1-repetition UCCSD is still able to approximate any of these three states. A more detailed description of the ability of the UCCSD ansatz to simultaneously represent an increasing number of excited states as the number of repetitions is increased is not yet known. qOMM could adopt many UCCSDs, UCCSD with many repetitions, or a mixture of them as its variational ansatz. SSVQE, however, could only benefit from increasing the repetitions in UCCSD. The second impact of ansatz circuit depth relates to optimization. Another field full of non-convex optimization and parametrized ansatz is the deep neural network. An interesting theoretical result³⁷ therein shows that enlarging the parameter space, *i.e.*, increasing the number of parameters, would make the optimization problem easier, *i.e.*, the energy landscape would be full of the approximated global minimum. Although we have not established similar results for quantum ansatz circuits, we observe the behavior from our numerical re-

sults. In Figure 7b, 1-repetition UCCSD is able to characterize the three states for LiH using qOMM. However, all ten random parameter initializations got stuck as in Figure 7a. As we increase the circuit depth from 1-repetition to 2-repetition UCCSD, qOMM rapidly converges to a global minimum for all ten random parameter initializations.

5 Conclusion

In this work we have proposed a method which can calculate the low-lying eigenvalue/eigenstate pairs of a Hermitian operator on quantum hardware. We have classically simulated the algorithm for two different electronic structure Hamiltonians: H_2 and LiH. We have compared it to SSVQE, another algorithm with the same goal, but one which enforces the orthogonality of the input states explicitly at every optimization step. We showed that a small problem such as H_2 is not difficult enough to meaningfully distinguish any differences in performance for these two approaches when using a random initialization strategy, but when one compares them to a more moderately-sized problem such as 10 qubit LiH, noticeable differences in performance begin to emerge. In this scenario, qOMM converges with fewer objective function evaluations and with lower ansatz circuit depth in all but one of the simulations considered here. It is worth re-iterating that these simulations are conducted in an ideal noiseless setting. These tests are a good first step as they can elucidate some information about what limitations are inherent to the algorithms and represent a best case scenario performance, but do not test how robust these algorithms are to realistic hardware noise. Testing these algorithms using realistic noise models and on real quantum hardware is one potential direction of future research.

These LiH simulations demonstrate that in the context of these types of excited states methods, even a crude initialization strategy can greatly reduce not only the number of optimization iterations needed to converge, but also the circuit depth needed to do so. Another po-

tentially interesting topic would be the extent to which these excited states methods could benefit from various adaptive ansatz methods that have been developed recently for ground state methods.^{38–40} Additionally, one could investigate whether or not modifying the SSVQE weight vector to adaptively change over the course of the optimization could mitigate the objective function plateau effect we observed in our simulations.

Acknowledgement The work is supported in part by the US National Science Foundation under award CHE-2037263 and by the US Department of Energy via grant DE-SC0019449.

References

- (1) Arute, F.; Arya, K.; Babbush, R.; Bacon, D. et al. Quantum supremacy using a programmable superconducting processor. *Nature* **2019**, *574*:7779 **2019**, *574*, 505–510.
- (2) Zhong, H.-S.; Wang, H.; Deng, Y.-H.; Chen, M.-C. et al. Quantum computational advantage using photons. *Science* **2020**, *370*, 1460–1463.
- (3) Blunt, N. S.; Smart, S. D.; Booth, G. H.; Alavi, A. An excited-state approach within full configuration interaction quantum Monte Carlo. *J. Chem. Phys.* **2015**, *143*, 134117.
- (4) Holmes, A. A.; Umrigar, C. J.; Sharma, S. Excited states using semistochastic heat-bath configuration interaction. *J. Chem. Phys.* **2017**, *147*, 164111.
- (5) Schriber, J. B.; Evangelista, F. A. Adaptive configuration interaction for computing challenging electronic excited states with tunable accuracy. *J. Chem. Theory Comput.* **2017**, *13*, 5354–5366.
- (6) Li, Y.; Lu, J.; Wang, Z. CoordinateWise descent methods for leading eigenvalue problem. *SIAM J. Sci. Comput.* **2019**, *41*, A2681–A2716.
- (7) Wang, Z.; Li, Y.; Lu, J. Coordinate descent full configuration interaction. *J. Chem. Theory Comput.* **2019**, *15*, 3558–3569.
- (8) Li, Y.; Lu, J. Optimal orbital selection for full configuration interaction (OptOrbFCI): Pursuing basis set limit under budget. *J. Chem. Theory Comput.* **2020**, *16*, 6207–6221.
- (9) Abrams, D. S.; Lloyd, S. Quantum algorithm providing exponential speed increase for finding eigenvalues and eigenvectors. *Physical Review Letters* **1999**, *83*, 5162–5165.
- (10) Aspuru-Guzik, A.; Dutoi, A. D.; Love, P. J.; Head-Gordon, M. Simulated quantum computation of molecular energies. *Science* **2005**, *309*, 1704–1707.
- (11) Peruzzo, A.; McClean, J.; Shadbolt, P.; Yung, M. H. et al. A variational eigenvalue solver on a photonic quantum processor. *Nature Communications* **2014**, *5*, 1–7.
- (12) Bauer, B.; Bravyi, S.; Motta, M.; Chan, G. K.-L. Quantum algorithms for quantum chemistry and quantum materials science. *Chemical Reviews* **2020**, *120*, 12685–12717.
- (13) McArdle, S.; Endo, S.; Aspuru-Guzik, A.; Benjamin, S. C. et al. Quantum computational chemistry. *Reviews of Modern Physics* **2020**, *92*, 015003.
- (14) McClean, J. R.; Kimchi-Schwartz, M. E.; Carter, J.; De Jong, W. A. Hybrid quantum-classical hierarchy for mitigation of decoherence and determination of excited states. *Phys. Rev. A* **2017**, *95*, 042308.
- (15) Colless, J. I.; Ramasesh, V. V.; Dahlen, D.; Blok, M. S. et al. Computation of molecular spectra on a quantum processor with an error-resilient algorithm. *Physical Review X* **2018**, *8*, 011021.

- (16) Ganzhorn, M.; Egger, D. J.; Barkoutsos, P.; Ollitrault, P. et al. Gate-efficient simulation of molecular eigenstates on a quantum computer. *Physical Review Applied* **2019**, *11*, 044092.
- (17) Ollitrault, P. J.; Kandala, A.; Chen, C.-F.; Barkoutsos, P. K. et al. Quantum equation of motion for computing molecular excitation energies on a noisy quantum processor. *Phys. Rev. Res.* **2020**, *2*, 043140.
- (18) McClean, J. R.; Romero, J.; Babbush, R.; Aspuru-Guzik, A. The theory of variational hybrid quantum-classical algorithms. *New J. Phys.* **2016**, *18*, 23023.
- (19) Santagati, R.; Wang, J.; Gentile, A. A.; Paesani, S. et al. Finding excited states of physical Hamiltonians on a silicon quantum photonic device. *Front. Opt.* 2017. 2017; p FM4E.2.
- (20) Santagati, R.; Wang, J.; Gentile, A. A.; Paesani, S. et al. Witnessing eigenstates for quantum simulation of Hamiltonian spectra. *Sci. Adv.* **2018**, *4*, eaap9646.
- (21) Higgott, O.; Wang, D.; Brierley, S. Variational quantum computation of excited states. *Quantum* **2019**, *3*, 156.
- (22) Jones, T.; Endo, S.; McArdle, S.; Yuan, X. et al. Variational quantum algorithms for discovering Hamiltonian spectra. *Phys. Rev. A* **2019**, *99*, 62304.
- (23) Nakanishi, K. M.; Mitarai, K.; Fujii, K. Subspace-search variational quantum eigensolver for excited states. *Physical Review Research* **2019**, *1*, 033062.
- (24) Parrish, R. M.; Hohenstein, E. G.; McMahon, P. L.; Martínez, T. J. Quantum computation of electronic transitions using a variational quantum eigensolver. *Physical Review Letters* **2019**, *122*, 230401.
- (25) Ordejon, P.; Drabold, D. A.; Grumbach, M. P.; Martin, R. M. Unconstrained minimization approach for electronic computations that scales linearly with system size. *Physical Review B* **1993**, *48*, 14646.
- (26) Mauri, F.; Galli, G.; Car, R. Orbital formulation for electronic-structure calculations with linear system-size scaling. *Physical Review B* **1993**, *47*, 9973.
- (27) Lu, J.; Thicke, K. Orbital minimization method with ℓ_1 regularization. *J. Comput. Phys.* **2017**, *336*, 87–103.
- (28) Byrd, R. H.; Lu, P.; Nocedal, J.; Zhu, C. A Limited Memory Algorithm for Bound Constrained Optimization. *SIAM Journal on Scientific Computing* **1995**, *16*, 1190–1208.
- (29) Kandala, A.; Mezzacapo, A.; Temme, K.; Takita, M. et al. Hardware-efficient variational quantum eigensolver for small molecules and quantum magnets. *Nature* **2017**, *549*, 242–246.
- (30) Gacon, J.; Zoufal, C.; Carleo, G.; Woerner, S. Simultaneous perturbation stochastic approximation of the quantum Fisher information. *Quantum* **2021**, *5*, 567.
- (31) Childs, A. M.; Wiebe, N. Hamiltonian simulation using linear combinations of unitary operations. *Quantum Info. Comput.* **2012**, *12*, 901–924.
- (32) Romero, J.; Babbush, R.; McClean, J. R.; Hempel, C. et al. Strategies for quantum computing molecular energies using the unitary coupled cluster ansatz. *Quantum Science and Technology* **2018**, *4*, 014008.
- (33) ANIS, M. S.; Abraham, H.; AduOfiei,; Agarwal, R. et al. Qiskit: An Open-source Framework for Quantum Computing. 2021.
- (34) Sun, Q.; Berkelbach, T. C.; Blunt, N. S.; Booth, G. H. et al. PySCF: the python-based simulations of chemistry framework. *Wiley Interdisciplinary Reviews: Computational Molecular Science* **2018**, *8*, e1340.
- (35) Gao, W.; Li, Y.; Lu, B. Triangularized orthogonalization-free method for solving extreme eigenvalue problems. 2020; <http://arxiv.org/abs/2005.12161>.

- (36) Gao, W.; Li, Y.; Lu, B. Global Convergence of Triangularized Orthogonalization-free Method. 2021; <https://arxiv.org/abs/2110.06212v1>.
- (37) Allen-Zhu, Z.; Li, Y.; Liang, Y. Learning and generalization in overparameterized neural networks, going beyond two layers. *Advances in Neural Information Processing Systems*. 2019.
- (38) Grimsley, H. R.; Economou, S. E.; Barnes, E.; Mayhall, N. J. An adaptive variational algorithm for exact molecular simulations on a quantum computer. *Nature Communications* **2019**, *10*, 1–9.
- (39) Tang, H. L.; Shkolnikov, V.; Barron, G. S.; Grimsley, H. R. et al. Qubit-ADAPT-VQE: An adaptive algorithm for constructing hardware-efficient ansätze on a quantum processor. *PRX Quantum* **2021**, *2*, 020310.
- (40) Yordanov, Y. S.; Armaos, V.; Barnes, C. H.; Arvidsson-Shukur, D. R. Qubit-excitation-based adaptive variational quantum eigensolver. *Communications Physics* **2021**, *4*, 1–11.